Dynamic aperture of electron storage rings with noninterleaved sextupoles

Katsunobu Oide and Haruyo Koiso
National Laboratory for High Energy Physics (KEK), Oho, Tsukuba, Ibaraki 305, Japan
(Received 29 June 1992; revised manuscript received 20 October 1992)

A detailed study of a dynamic aperture is given for electron storage rings with noninterleaved sextupole magnets. As a result of a cancellation of major transverse nonlinearities of sextupoles by $-I$ transformers, other tiny terms such as fringe fields of quadrupoles and kinematical terms of drift spaces come to limit the transverse dynamic aperture. Results for transverse aperture in simulations can be explained by a simple one-dimensional model including these terms. In the longitudinal direction, a modulation of linear betatron motion by synchrotron oscillation is investigated as the source of the aperture limit.

PACS number(s): 41.85.Gy, 29.27.−a, 29.20.Dh

I. INTRODUCTION

The dynamic aperture is one of the major issues in electron storage ring design for high-energy colliders, small-emittance light sources, and damping rings for linear colliders. If a storage ring consists of only nearly linear elements such as drift spaces and dipole and quadrupole magnets, one may expect a large dynamic aperture for transverse (betatron) motion around the equilibrium orbit. Unfortunately this is only true for a particle at the design momentum of the ring, since the focusing strengths of magnets are always inversely proportional to the momentum of a particle due to the nature of the Lorentz force. This change of focusing due to the momentum deviation from the design momentum is called *chromaticity*. The chromaticity of a ring shifts the betatron tune, which is the number of betatron oscillations in one turn, for off-momentum particles. Eventually the chromaticity leads the particles into integer or half-integer resonances which blow up the amplitude of the betatron oscillation. The linear chromaticity of betatron tunes $\xi_{x,y}$ is the most significant of all chromatic effects of the ring. It is defined as the change of the betatron tune $\Delta\nu_{x,y}$ divided by the relative momentum change of a particle $\chi \equiv \Delta p/p$. We use x and y to denote the horizontal and vertical directions of the betatron motion. The linear chromaticity of focusing elements in a ring is expressed as

$$\xi_{x,y}=\frac{\partial\nu_{x,y}}{\partial\chi}=-\frac{1}{4\pi}\int K(s)\beta_{x,y}(s)ds \ , \tag{1}$$

where $K(s)$ is the focusing strength and $\beta_{x,y}(s)$ the beta function, and both are functions of the position s on the design orbit around the ring. The magnitude of $\xi_{x,y}$ is determined by the linear beam optics, and becomes large when the focusing is strong.

To avoid the resonances caused by the chromaticity one needs to perform *chromaticity correction* by putting correctors in a ring. A classical method of chromaticity correction is to place sextupole magnets at locations where the horizontal dispersion is not zero. Horizontal dispersion is naturally created by the bending magnets in the arc of the ring, so the sextupoles are usually distributed in the arc. A thin sextupole magnet kicks a particle according to

$$\Delta x'=-k'[(x+\eta\chi)^2-y^2]/2, \quad \Delta y'=k'(x+\eta\chi)y \ , \tag{2}$$

where $\Delta x'$ and $\Delta y'$ are the changes of the angle, η is the horizontal dispersion, and $k'=\int K'ds$ is the integrated strength of the sextupole. The terms $-k'x\eta\chi$ and $k'y\eta\chi$ in Eq. (2) function as chromatic lenses and accomplish the chromaticity correction. Therefore the sextupoles give linear chromaticities

$$\xi_{x,y}=\frac{1}{4\pi}\int K'(s)\beta_{x,y}(s)\eta(s)ds \ . \tag{3}$$

It is possible to choose the strength $K'(s)$ properly to cancel Eq. (1) by Eq. (3) in both x and y planes. Although the sextupoles correct the linear chromaticities easily, this method induces several undesirable effects. The principal effect is the nonlinear transverse kick written in Eq. (2), which is the major source of transverse nonlinearity and the resulting higher-order resonances. Combinations of nonlinear kicks by all sextupoles in a ring are also important.

The best way to remedy the nonlinearity of the sextupole is to make a pair of two identical sextupoles which are connected by a $-I$ transformer both in the x and y planes. The parity of the kicks in Eq. (2) reveals that all nonlinearities are canceled if the signs of positions and angles are reversed by the $-I$ transformer [1]. The effect for the chromaticity correction still remains if we put dipoles inside the $-I$ to make equal dispersions at the two sextupoles. The performance of the $-I$ transformer scheme becomes most efficient in the noninterleaved scheme which eliminates other sextupoles within the $-I$. The reason is that in an interleaved $-I$ scheme, coupling terms between sextupoles remain and are as important as the single sextupole nonlinearities. This noninterleaved method has been applied in designs of final focus systems of future linear colliders [2] which require nanometer spot sizes at least in one dimension at the focal point. Works for storage rings also have been performed by the other authors [3], and this study is an extension of their

works using a design of a B-meson factory as an example.

Another problem in the chromaticity correction is the nonlocality of the sources of chromaticities including the correctors. In the case of a high luminosity collider the natural sources of chromaticity concentrate in the insertions around an interaction point (IP), while the correctors are placed in the arc. In this situation the two distant chromatic sources, even though they are canceling each other, generate higher-order chromatic effects through the small chromaticity of the beam line between them. The phase relations between correctors also produce higher-order terms in the chromaticity. Later we will discuss examples where such higher-order chromaticities limit the momentum acceptance of the ring through couplings between the longitudinal (synchrotron) and the betatron motions. The magnitude of the higher-order chromaticity strongly depends on the choice of the strengths of the sextupoles and their optical locations. Generally speaking, the number of families of sextupoles is a practical key to increasing the momentum acceptance.

The noninterleaved scheme has many merits for storage ring design. The machine becomes so nearly linear in the transverse dimensions that we greatly improve the acceptance for the injected beam. A large aperture not only results in a high injection efficiency, but protects detectors from the tail of the injected beam hitting them. It also increases the lifetime of the beam because it holds large-amplitude particles scattered by particle-particle, beam-beam, intrabeam, and particle-gas interactions. After the cancellation of the transverse nonlinearity of the sextupoles, the transverse dynamic aperture in the noninterleaved sextupole scheme comes to be limited by other tiny nonlinearities at least for particles around the design momentum. In Sec. III, we will show that the fringe field of the final quadrupoles and so-called kinematical effects in the drift space at the IP give a definite limit on the vertical dynamic aperture in the case of a collider with small β-function insertions.

Generally speaking, the noninterleaved scheme has large higher-order chromaticities compared to the interleaved, because it has fewer and more nonuniformly distributed sextupoles. We will show that the main reason that limits the momentum acceptance of the noninterleaved scheme is a modulation of the linear betatron motion by synchrotron oscillations coupled through the higher-order chromaticities. This paper will show that the acceptance in the longitudinal direction becomes as good as the interleaved scheme, if a sufficient number of sextupole families are put in the ring and also if the machine tune is chosen so as to avoid the modulation resonances.

II. DYNAMIC APERTURE WITH NONINTERLEAVED SEXTUPOLES

Hereafter we use the term "dynamic aperture," or "dynamic acceptance," to mean a set of initial conditions of a particle which circulates stably in a storage ring for a certain large number of turns. Since an electron ring has a damping of oscillations around the equilibrium orbit due to synchrotron radiation, the dynamic aperture should be defined as a stability for one damping time, which typically ranges from a few hundred to a few thousand turns. This situation is much different from that in a proton ring where stability for a few million turns has been discussed [4]. In other words, an electron ring can accept a particle whose amplitudes and nonlinearities are much larger than a proton ring. The strong nonlinearity makes the analysis of the dynamic aperture of an electron ring difficult, and a perturbation method easily fails. On the other hand, it is not difficult to estimate the dynamic aperture by a simple particle-tracking simulation because of the short number of turns. Therefore, in this study we mainly use results of tracking to evaluate the dynamic aperture.

We use six canonical variables x, p_x, y, p_y, z, and δ to describe the motion of a particle. The independent variable is the location s on the design orbit. Variables p_x and p_y are transverse canonical momenta normalized by the design momentum p_0. The longitudinal variable z is defined as $z \equiv -vt$, where t is the difference of the arrival time from the reference time at the location s. The last variable is the relative momentum difference $\delta = \Delta p / p_0$. The Hamiltonian through the ring is written as [5]

$$H = -\left[1+\frac{x}{\rho}\right]\{[(1+\delta)^2-(p_x-eA_x/p_0)^2 -(p_y-eA_y/p_0)^2]^{1/2}+eA_s/p_0\} +\frac{c}{v_0}[(1+\delta)^2+(mc/p_0)^2]^{1/2}, \quad (4)$$

where ρ is the horizontal bending radius, (A_x, A_y, A_s) the vector potential of magnets and rf cavities, and v_0 the design velocity at the design momentum. We have neglected terms of vertical bending magnets and the electrostatic potential because we do not have them in the model ring in this paper. Although the number of turns for tracking is small, it takes considerable computer power to survey the entire six-dimensional phase space of the initial condition of a particle. In this paper we limit the initial conditions to $p_{x0}=0$, $p_{y0}=0$, $z=0$, and $y=ax$, where a is a constant. We usually choose a so that the initial value of action J_{y0} is always equal to J_{x0}. The action J_x is defined by the Courant-Snyder invariant

$$2J_x = \beta_x(s)[p_x + x\alpha_x(s)/\beta_x(s)]^2 + x^2/\beta_x(s), \quad (5)$$

which is a constant in the limit of linear betatron motion. We define J_y similarly. We carry out the tracking by a code named SAD [6], which performs fully symplectic transformations in six dimensions. Synchrotron radiation is neglected in the tracking. Our criterion for stability is that x and y never exceed 10 cm, roughly the physical aperture of a typical ring, during 1000 turns of tracking. The dynamic aperture does not depend strongly on the precise numbers for the criterion, since particle loss is typically the result of exponential growth of the amplitudes. As an example for this study, we select a ring designed for the asymmetric B-meson factory in the TRISTAN [10] tunnel. Table I shows the main charac-

TABLE I. Machine parameters of the model ring.

Beam energy	E	3.5 GeV
Circumference	C	3010 m
Betatron tunes	ν_x	39.12
	ν_y	39.15
Synchrotron tune	ν_z	0.049
Horizontal emittance	ϵ_x	1.86×10^{-8} m
Bunch length	σ_z	6.7 mm
Momentum spread	σ_δ	7.8×10^{-4}
Momentum compaction factor	α_p	8.9×10^{-4}
Momentum damping period	$c\tau_\delta/C$	3950 turns
Beta functions at the IP	β_x^*	1 m
	β_y^*	0.01 m
Chromaticities	ξ_x	-61
	ξ_y	-87

teristics of the model ring.

First we show in Fig. 1 comparison of dynamic apertures obtained by tracking for the noninterleaved and the interleaved schemes. The vertical axis is the transverse acceptance for the initial condition, expressed in terms of the initial actions (a) $J_{x0}=J_{y0}$ and (b) $J_{x0}=10J_{y0}$. The horizontal axis is the initial momentum deviation δ_0. We see a big improvement in the transverse acceptance with the noninterleaved scheme, keeping the longitudinal acceptance almost unchanged. The reason that the improvement is greater in (b) than in (a) is that in the noninterleaved scheme the dynamic aperture is limited in the vertical plane by residual nonlinearities around the IP.

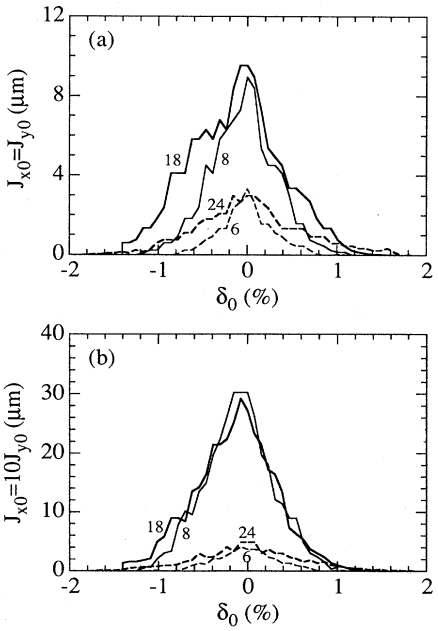

FIG. 1. Comparison of the dynamic aperture of the noninterleaved (solid) and interleaved (dashed) schemes. The numbers at the curves show the number of sextupole families. When the initial vertical action is $\frac{1}{10}$ of the horizontal (b), the difference of the two schemes is larger than in case (a).

We discuss the mechanism in Sec. III. Although the result depends on machine tunes as we discuss later, for most tunes we get an improvement in the transverse acceptance of at least a factor of 2.

Figure 1 also shows the dependence of the dynamic aperture on the number of the sextupole families. For both schemes a larger number of families brings a wider momentum acceptance, with no damage in the transverse direction. In the case of the model ring, the noninterleaved scheme has a unit cell of $\pi/2$ phase advance in both x and y planes in the arc. This structure is suitable for placing as many of the sextupole families as possible. The maximum number of the families for the model ring is limited to 18 by the size of the arc. Each family consists of four sextupoles, since this ring has a mirror symmetry around the IP. The interleaved has a $\pi/3$ unit cell, where each quadrupole accompanies a sextupole. Sextupoles of π phase differences are paired to cancel their lowest order of the transverse nonlinearity to each other. The interleaved scheme has a maximum of 24 families of 288 sextupoles. In the rest of this study we use 18 families as the standard of the noninterleaved scheme.

The dynamic aperture greatly depends on the choice of strengths of the sextupole families. In the case of the noninterleaved scheme the transverse nonlinearities are small and, consequently, we can concentrate on widening the longitudinal aperture. This model ring has one rf section on the opposite side of the IP, where the ring has a mirror symmetry. The algorithm we apply here is to find a solution which minimizes the deviation of transverse tunes $\nu_{x,y}$ and beta functions $\beta_{x,y}^{\rm rf}$ at the midpoint of the rf cavity section, for a given range of the momentum deviation $-\delta_1<\delta<\delta_1$. The Twiss parameters $\alpha_{x,y}^{\rm rf}$ area always zero because of the symmetry. If we assume that a particle changes its momentum only at the rf section, the oscillation becomes stable in the case that the linear one-turn map from the rf is insensitive to δ. Actually the change of energy due to the radiation in the arc is the order of δ/(damping turns), which is smaller than the change by the rf, $\delta/2\pi\nu_z$. Thus the assumption above is well justified. We choose seven points of different momenta within $\pm1.6\%$ in this study, and minimize the deviations of $\nu_{x,y}$ and $\beta_{x,y}^{\rm rf}$ at these momenta by varying the sextupole strengths. Figure 2 shows the residual deviations of these functions.

This study has applied the same algorithm to determine the strengths of sextupoles both in the noninterleaved and interleaved schemes. In the case of the interleaved scheme there may exist thousands of methods to find a good solution [7], but no universal formula is known yet. Difficulties come from the mixture of all transverse nonlinearities and higher-order chromaticities. In our view the noninterleaved scheme has a great merit since it separates the transverse problems from the chromatic ones. The algorithm for the noninterleaved scheme described above is quite simple, yet sufficient to achieve a practical performance of the dynamic aperture. Note that the result in Fig. 2 is a comparison between two schemes with solutions obtained by the same specific algorithm. We do not deny a possibility of other solutions which increase the aperture for both schemes.

Another point we have studied is the significance of the synchrotron motion. We expect that the noninterleaved scheme has two major sources which limit the dynamic aperture of off-momentum particles. One is a breakdown of the $-I$ transformation of sextupole pairs due to the momentum deviation, and another is a modulation of the transverse motion by the synchrotron oscillation. To see these effects, first we turned off the synchrotron motion in the tracking by setting the rf voltage to zero. The result in Fig. 3 shows that the dynamic aperture for off-momentum particles is strongly affected by the synchrotron motion. In Sec. IV we identify the cause to be modulation of the betatron oscillation by the synchrotron motion. The effect of the synchro-betatron resonances is larger in the noninterleaved scheme than in the interleaved one. The reason is that the higher-order chromaticities of noninterleaved are stronger than interleaved as shown in Fig. 2.

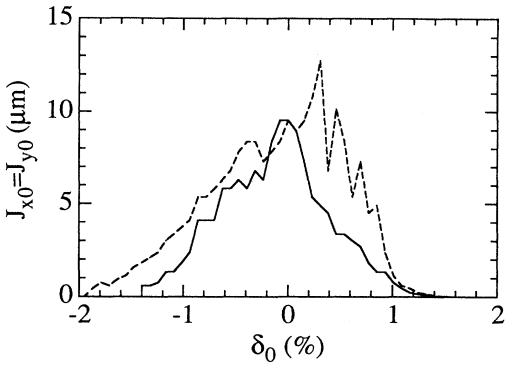

FIG. 3. The dynamic aperture for off-momentum particles for the noninterleaved scheme worsens in the presence of the synchrotron motion. The solid line is the aperture with synchrotron motion and dashed without.

It is natural to guess that the performance of the noninterleaved scheme may be damaged by the machine errors which disturb the $-I$ transformation. We have studied the effect on dynamic aperture of errors in quadrupole and sextupole strengths. Figure 4(a) shows the change in the dynamic aperture for 12 random errors of

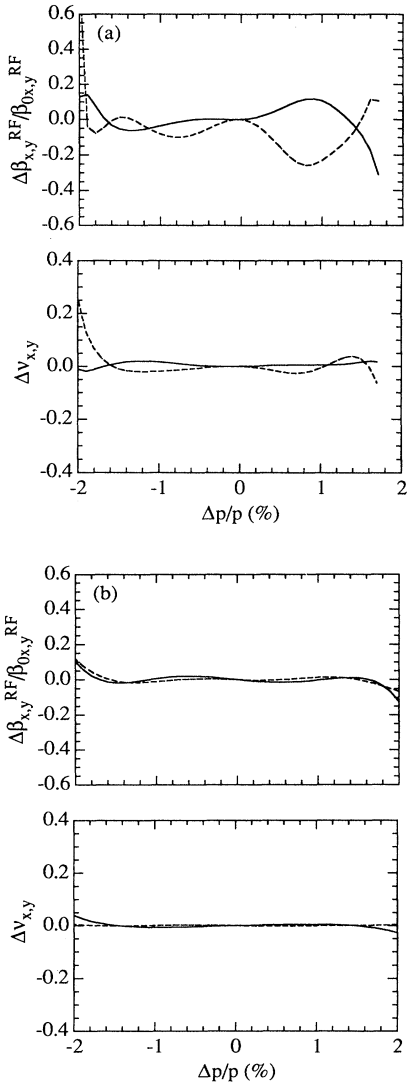

FIG. 2. Sextupoles are chosen to minimize the relative variation in the β functions $\beta_{x,y}^{rf}$ at the midpoint of the rf section and the betatron tunes $\nu_{x,y}$ due to momentum deviations $\Delta p/p$. The results depend on the (a) noninterleaved or (b) interleaved schemes. The solid lines correspond to the horizontal functions and the dashed to the vertical.

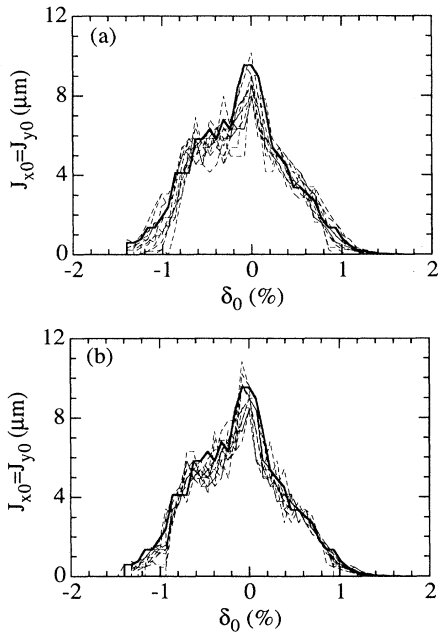

FIG. 4. The dynamic aperture in the presence of machine errors for the noninterleaved scheme. (a) Strength errors of the quadrupoles and the sextupoles: The dashed lines correspond to 12 different random numbers for 0.1% relative strength errors. (b) Misalignments of sextupoles: The dashed lines correspond to 12 different random numbers for 100-μm transverse and 200-μm longitudinal misalignments. The solid line is the aperture without errors.

0.1% relative strength errors applied to all quadrupoles and sextupoles in the ring. These errors have Gaussian distributions with 3σ cutoff. In these simulations with errors, we have adjusted the transverse tunes each time by varying quadrupoles in the same way as the actual machine operation, because the measurement and correction of tunes are easily done with an enough accuracy. The decrease of the aperture still looks acceptable, especially in the transverse directions, since such a strength error less than 0.1% is not difficult to achieve with conventional technologies. We speculate that the strength error plays a roll somewhat similar to the momentum deviation of a particle. A relative strength error ϵ in magnets has nearly the same effect as an off-momentum particle of $\delta \sim \epsilon$, or even better than that because of the randomness. In the dynamic aperture without errors in Fig. 4(a), we see that the drop in the dynamic aperture for $\delta = \pm 0.1\%$ is consistent with the result with strength errors. We have also checked the effect of alignment errors of sextupoles on the dynamic aperture as shown in Fig. 4(b). The performance of the noninterleaved scheme is not very sensitive to the misalignments.

III. TRANSVERSE DYNAMIC APERTURE

The noninterleaved scheme appears capable of removing the major transverse nonlinearities which are usually induced by sextupoles. In this section we discuss the remaining sources of nonlinearities, which are hidden beneath sextupoles in the interleaved scheme. In the noninterleaved scheme these tiny nonlinearities come to limit the transverse dynamic aperture at least for particles with small amplitudes of synchrotron motion around the design momentum. For the time being we concentrate on pure geometric terms. In an electron-positron colliding machine with low β-function insertions, the vertical dynamic aperture is much smaller than the horizontal one because of a flat beam scheme with a strong vertical focusing. In such cases for a particle which has equal x and y amplitudes of the initial condition, the horizontal and coupled nonlinearities do not contribute much to the entire dynamic aperture so long as the machine tunes are not close to coupling resonances.

In the case of a high luminosity collider with a low β-function insertion at the IP, the residual vertical nonlinearity mainly comes from two sources around the IP. The first one is a nonlinear fringe field at the edges of the final quadrupole magnet. The change of the main transverse component of the magnetic field along the orbit always accompanies higher-order longitudinal and transverse magnetic fields at the edges to satisfy the Maxwell equations. Although the form of these higher-order fields depends on the actual design of the magnet, a sharp edge model is a good approximation to estimate their effects at a design stage of a ring. A sharp edge of a quadrupole magnet which has a step function for the primary focusing field induces a higher-order effect expressed by an effective Hamiltonian [8]

$$H_{\pm} = \pm \frac{K}{1+\delta} \left[\frac{u\bar{u}^2 p_u}{8} - \frac{u^3 p_u}{24} \right] \delta_C(s - s_e) + \text{c.c.} , \tag{6}$$

where K is the strength of the quadrupole, s_e the location of the edge, and δ_C the periodic delta function with the period of the machine circumference C. The positive sign is chosen at the entrance and the negative at the exit. We have also introduced the canonical variables $u \equiv x + iy$ and $p_u \equiv (p_x - ip_y)/2$. If we concentrate on the vertical motion at the design momentum, Eq. (6) is reduced to

$$H_{\pm} = \mp \frac{K y^3 p_y}{12} \delta_C(s - s_e) . \tag{7}$$

The major fringes are the two inside edges, facing the IP, of the final quadrupoles. The Hamiltonians at those edges are translated to a Hamiltonian at the IP ($s = 0$) by replacing y and p_y in Eq. (7) with variables at the IP as $y = y^* \pm l^* p_y^*$ and $p_y = p_y^*$, where l^* is the distance between the IP and the quadrupole face. The total effect of the two fringes is expressed as

$$\begin{aligned} H_f &= H_+ + H_- + O(K^2) \\ &= -\frac{K}{6}(3y^{*2} p_y^{*2} l^* + p_y^{*4} l^{*3}) \delta_C(s) + O(K^2) \\ &\approx -\frac{K}{6} p_y^{*4} l^{*3} \delta_C(s) , \end{aligned} \tag{8}$$

where we have neglected the higher orders of K and used $p_y^* l^* \gg y^*$. The last relation comes from $l^* \gg \beta_y^*$.

The second source of the residual nonlinearity is the so-called kinematical effect. The general Hamiltonian (4) of a particle in a ring always has transverse nonlinear terms which come from the expansion of the first square root even in a drift space. We write the Hamiltonian of a drift space up to the fourth order:

$$H = -1 - \delta + \frac{p_x^2 + p_y^2}{2(1+\delta)} + \frac{(p_x^2 + p_y^2)^2}{8(1+\delta)^3} . \tag{9}$$

In the vertical plane this effect is also strong in the drift space around the IP. We can translate the integrated effect of the nonlinear part in Eq. (9) over the drift space of length $2l^*$ into a Hamiltonian at the IP, and obtain

$$H_k = \frac{p_y^{*4} l^*}{4} \delta_C(s) , \tag{10}$$

where we have picked only the vertical term at the design momentum. The nonlinearity in a drift space may sound strange, because the map for (x, x', y, y') in a drift space is linear. A question arises whether there is a merit to remove the nonlinearity by choosing (x, x', y, y') as the variables instead of the usual canonical variables (x, p_x, y, p_y). The answer is negative, since the map of the rest of the ring for (x, x', y, y') becomes no longer symplectic in electromagnetic fields. Therefore the picture with (x, x', y, y') looks even more difficult in the map of the rest of the ring. The canonical view of a drift space with the kinematical nonlinearity is consistent and preferable.

Since the nonlinear Hamiltonians (8) and (10) have the same form, we can simply add them to get the total effect. If we assume the rest of the ring is completely linear, the total Hamiltonian for the ring is written as

$$H=H_f+H_k+J_y\mu_y/C$$
$$=(1-\tfrac{2}{3}Kl^{*2})\frac{l^*J_y^2}{\beta_y^{*2}}\cos^4\psi_y\delta_C(s)+J_y\mu_y/C\ , \qquad (11)$$

where we have used action-angle variables defined as $y^*=(2J_y\beta_y^*)^{1/2}\sin\psi_y$ and $p_y^*=(2J_y/\beta_y^*)^{1/2}\cos\psi_y$. We can scale J_y and H as

$$J_y'=(1-\tfrac{2}{3}Kl^{*2})\frac{l^*J_y}{\beta_y^{*2}},\quad H'=\frac{J_y'}{J_y}H\ , \qquad (12)$$

and rewrite Eq. (11) to

$$H'=J_y'^2\cos^4\psi_y\delta_1(n)+\mu_yJ_y'\ , \qquad (13)$$

where the independent variable is changed from s to the number of turns n. The aperture of the motion is now described by a simple one-dimensional Hamiltonian (13), which has only one parameter μ_y. We estimated the stable region of the motion determined by the Hamiltonian (13) by a simple mapping started at $J_y'=J_{y0}'$, and obtained the aperture $A(\mu_y)$ for J_{y0}' as a function of μ_y. The shape of $A(\mu_y)$ is shown in Fig. 5 for $0<\mu_y/2\pi<0.5$. The same pattern is repeated in the range $0.5<\mu_y/2\pi<1$. One can easily see from Eq. (13) that the perturbed tune increases when the amplitude becomes larger. The pattern in Fig. 5 is basically determined by this positive tune shift and the second, fourth, and sixth resonances. There are three dips on the curve of $A(\mu_y)$ in Fig. 5 at $\mu_y/2\pi=0.11$, 0.22, and 0.30. These dips correspond to formation of a Kolmogorov-Arnold-Moser (KAM) surface surrounding the sixth and fourth resonance islands around the stable region. If the tune becomes higher than the dips, a KAM surface is formed to enclose these islands and the stable region is enlarged. Figure 6 shows this situation for the sixth-order resonance around $\mu_y/2\pi=0.11$. These dips are also seen in the results of the full tracking. The aperture for the original action J_{y0} is written as

$$J_{y0}=\frac{\beta_y^{*2}}{(1-2Kl^{*2}/3)l^*}A(\mu_y)\ . \qquad (14)$$

Note that the sign of K is negative because the final quadrupole is vertically focusing.

Figure 5 shows good agreement between the estimation (14) and the results of the full tracking. The results by tracking are converted into $A(\mu_y)$ using Eq. (14). In this case the parameters are $K=-1.4\ \mathrm{m}^{-2}$ and $l^*=1.5$ m, and the contribution of the fringe term is 2.1 times larger than that of the kinematical terms. The result in the dashed curve ($J_{x0}=0$) agrees very well with Eq. (14) (solid). Even the dotted results ($J_{x0}=J_{y0}$) show similar characteristics. We set $\mu_x/2\pi=0.12$ in the case of Fig. 5 for the full tracking. We find that Eq. (14) is applicable for β_y^* as large as 2 cm, provided $J_y\sim30$ μm.

We have also studied the effect of the thickness of sextupoles. The thickness of a sextupole gives a higher-

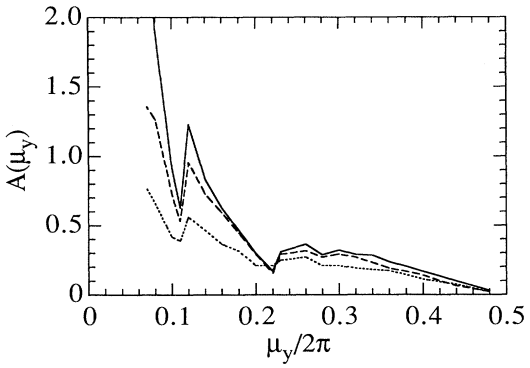

FIG. 5. The transverse dynamic aperture, especially in the vertical plane, is determined by the fringe field of the final quadrupole at the IP and the kinematical term in the drift space at the IP. The aperture is given by a universal function $A(\mu_y)$ (solid) determined by a simple one-dimensional model. The dashed line is the result of full tracking with zero initial horizontal amplitude, and the dotted curve corresponds to equal initial horizontal and vertical amplitudes.

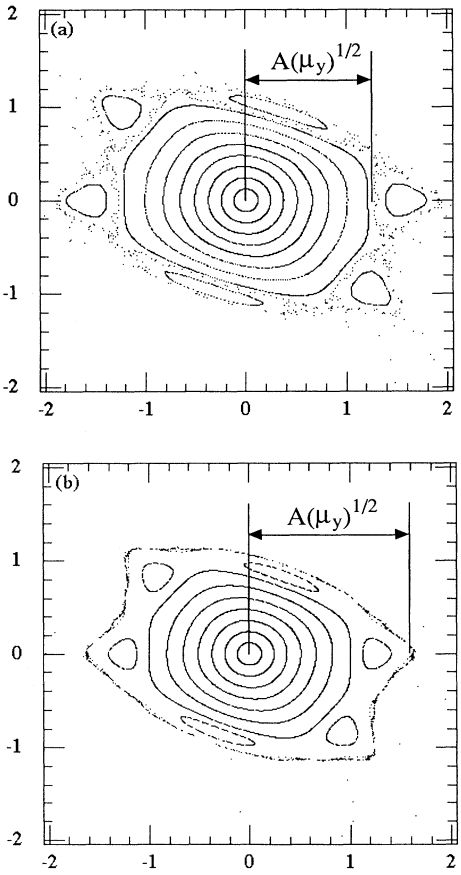

FIG. 6. The phase space plot of (J_y',ψ_y) with the Hamiltonian of Eq. (13). (a) At $\mu_y/2\pi=0.105$ the area between the sixth-order islands and the main stable area is not stable. (b) At $\mu_y/2\pi=0.117$ the sixth-order island is surrounded by a KAM surface and the aperture becomes larger than in (a). This change of aperture corresponds to the dips of Fig. 5.

order term which is not canceled by the $-I$ transformer as

$$H_t=\sum_i -\frac{k_i'^2 l_i}{48}(x^2+y^2)^2\delta_C(s-s_i)\ , \tag{15}$$

where k_i', l_i, and s_i are the integrated strength, the thickness, and the location of the ith sextupole. In Eq. (15) we have shown only the first-order term in l_i. The transverse aperture near the design momentum increases as the sextupoles become thicker. The reason is that the thickness brings a negative transverse tune shift due to the transverse oscillation amplitude. The negative tune shift somewhat cancels the positive tune shift caused by the nonlinear terms in (11), and thus increases the aperture. The amplitude dependent tune shift is $\Delta\nu_y/J_y=+0.0056$ and $-0.0012\ \mu\text{m}^{-1}$ for (11) and (15) (with the original thickness), respectively. In the model ring the thickness of the sextupoles is 15 or 20 cm. We did tracking simulation with different thickness of sextupoles. It results that the vertical aperture near the design momentum is decreased by about 20% by making the thickness of all sextupoles zero. If we double the thickness of all sextupoles, the vertical aperture increases by about 30%. The longitudinal acceptance does not change significantly by the thickness.

IV. MODULATION OF LINEAR BETATRON OSCILLATIONS

In this section we concentrate on the momentum acceptance for particles which have large momentum deviations and small betatron amplitudes for initial conditions. In the noninterleaved sextupole scheme, the momentum acceptance is limited by several factors. One is the natural acceptance $\pm\delta_1$ of the chromaticity correction which we use during the search for the sextupoles. Beyond $|\delta|>\delta_1$ the linear map for an off-momentum particle becomes unstable, as shown in Fig. 2. This acceptance basically depends on the magnitudes of higher-order chromaticities produced by the sextupoles, and also the number of sextupole families. It is not easy to give a rigorous expression for the acceptance, but roughly speaking a larger number of sextupole families gives a wider range of stability. We have already seen an example of the effect of the number of families in Fig. 1.

Another serious point for the momentum acceptance is the modulation of the linear betatron motion by the synchrotron oscillation. As the residual of the chromaticity correction, there still remains a small deviation of the β functions that causes a change of the one-turn linear map for an off-momentum particle. Every time a particle passes the rf section, the change of the momentum by the cavities produces a mismatch of the particle and the betatron ellipse in the phase space due to the change in the β function. The amplitude of the betatron oscillation changes according to

$$\begin{aligned}\Delta J_{x,y}&=J_{x,y}\frac{\Delta\beta^{\text{rf}}_{x,y}(\delta)}{\beta^{\text{rf}}_{x,y}}\cos 2\psi_{x,y}\ ,\\ \Delta\psi_{x,y}&=-\frac{\Delta\beta^{\text{rf}}_{x,y}(\delta)}{2\beta^{\text{rf}}_{x,y}}\sin 2\psi_{x,y}\ ,\end{aligned} \tag{16}$$

where $\Delta\beta^{\text{rf}}_{x,y}$ is the change of the beta function at the rf due to the change of the momentum deviation δ. We have assumed that the ring has only one rf section at s_{rf}, and neglected terms of higher-order than $O((\Delta\beta^{\text{rf}}_{x,y})^2)$. The transformation of Eq. (16) is also derived from a Hamiltonian

$$H=-\frac{J_{x,y}\Delta\beta^{\text{rf}}_{x,y}(\delta)}{2\beta^{\text{rf}}_{x,y}}\delta_C(s-s_{\text{rf}})\sin 2\psi_{x,y}\ . \tag{17}$$

If we neglect subsequent perturbation of the synchrotron motion by the perturbed betatron motion, important only when the betatron amplitude is large, the synchrotron phase ψ_z becomes proportional to the number of turns n as $\psi_z=2\pi n\nu_z$, and also its amplitude becomes constant, i.e., $\delta=\delta_0\sin 2\pi n\nu_z$. The betatron phase $\psi_{x,y}$ contains both the main term $2\pi n\nu_{x,y}$ and the chromaticity term $\int 2\pi\,\Delta\nu_{x,y}dn$, but we neglect the latter which only gives a second order term in Eq. (17). The form of $\Delta\beta^{\text{rf}}_{x,y}(\delta)$ results from the chromaticity correction and has many terms if expanded in a Fourier series of $2\pi n\nu_z$. Therefore the Hamiltonian (17) has resonances at

$$2\nu_{x,y}\pm m\nu_z=N\ , \tag{18}$$

where m and N are integers. These resonances induce an exponential growth of $J_{x,y}$, because the change of $J_{x,y}$ is proportional to $J_{x,y}$ as shown in Eq. (16).

Figure 7 shows the momentum acceptance δ_0 as a function of ν_z obtained by tracking and also a linear mapping method based on Eq. (16). We performed the linear mapping as follows. First we assumed the synchrotron motion is sinusoidal, $\delta=\delta_0\sin 2\pi n\nu_z$. Next we obtained linear betatron maps on a grid in δ of width $\pm 3\%$, with a 0.1% mesh size, and interpolated the map using the value at this mesh. The interpolation is performed for ten parameters to describe 4×4 symplectic matrices, so the interpolated map is always 4×4 symplectic. We used a cubic spline for the interpolation. The result of the tracking in Fig. 7 exhibits the resonances $2\nu_{x,y}\pm m\nu_z=N$ given by the modulation, and the linear map method gives an answer close to the tracking. The agreement between methods confirms that the modulation of the linear betatron motion is the dominant source limiting the momentum acceptance of the noninterleaved scheme. In Fig. 7 the dips in the acceptance at the resonances look milder than those predicted by the linear mapping method. One speculation is that the transverse nonlinearity in the lattice may smear the resonance through the amplitude dependence of the betatron tunes. The dips look even milder in y plane, which is due to the fact that the y tune shift is five times larger than in the x plane.

There is an additional effect from the dependence of

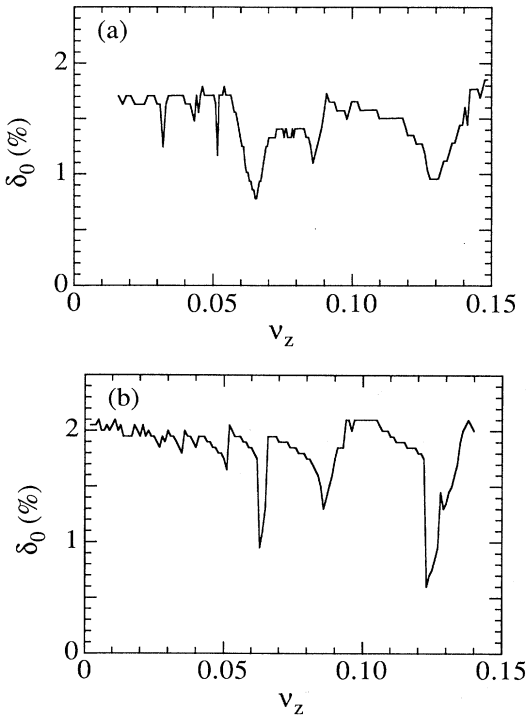

FIG. 7. The momentum acceptance depends on the synchrotron tune ν_z. The betatron tunes are $\nu_x = 39.12$ and $\nu_y = 39.15$. At resonances $2\nu_{x,y} \pm m\nu_z = N$ there are significant dips in the acceptance. (a) is the result of the full tracking, and (b) the linear off-momentum mapping.

the linear map on the synchrotron motion: the fixed point of an off-momentum linear map changes as a function of the momentum deviation. In a usual design the linear dispersion at the rf section is suppressed, but the higher-order dispersions still remain. The change of the momentum at the rf shifts the origin of the betatron oscillation in every turn, and continually excites the betatron motion through the synchrotron coupling. This effect, however, is less significant than the modulation effect discussed in the preceding paragraphs, since it does not give an exponential growth and is balanced by radiation damping. We have also included this effect in the linear mapping of Fig. 7(b).

Looking at Fig. 7, we find in the region $\nu_z \lesssim 0.02$ that the effect of the modulation is weak and the dynamic aperture is not much affected by the choice of the tunes. The reason is that since the synchrotron tune is small, the order of the resonance $m\nu_z$ must be high to satisfy the resonant condition (18), and the magnitude of the modulation Hamiltonian (17) decreases. From this point of view, a better way to design a machine would be to make ν_z as small as possible. On the other hand, there is a simple relationship between the bunch length σ_z and the momentum spread σ_δ of an electron storage ring [9]:

$$\sigma_z \approx \frac{c\alpha_p}{\nu_z \omega_0} \sigma_\delta , \tag{19}$$

where ω_0 is the revolution angular frequency of the ring. The parameter α_p, the momentum compaction factor, is the ratio of the orbit dilation $-\Delta z$ around the ring to the momentum deviation, i.e., $\Delta z / C = -\alpha_p \delta$, where C is the circumference. Thus the only one way to decrease ν_z while keeping σ_z, σ_δ, and C constant is to make α_p small. The momentum compaction factor α_p is expressed as

$$\alpha_p = \frac{1}{C} \int_0^C \frac{\eta}{\rho} ds , \tag{20}$$

and basically determined by the structure of the unit cell in the arc of the ring. Equation (20) shows that α_p is reduced if the horizontal dispersion η is small in bending magnets of the arc. Such a periodic structure can be made by putting bending magnets at every π horizontal phase advance. This structure is also suitable for the noninterleaved sextupole scheme because it can place the $-I$ sextupoles efficiently, if we make the vertical as well as horizontal phase advance per unit cell equal to π. Besides the dynamic aperture issue, a ring with small ν_z and α_p has the merit that the accelerating voltage is low, since the accelerating voltage is proportional to α_p if we keep the bunch length and the momentum spread constant.

V. CONCLUSIONS

The chromaticity correction with the noninterleaved sextupole scheme dramatically improves the dynamic aperture in the transverse direction. The machine looks so linear in the transverse direction that only tiny residual nonlinearities such as fringe fields of quadrupoles and kinematical terms of drift spaces limit the dynamic aperture. We derived a formula (14) for the transverse dynamic aperture near the design momentum. This formula is applicable to the case of a ring has with a low β-function insertion with strong vertical focusing. The dynamic aperture in the momentum direction including the synchrotron motion is made satisfactory if the number of families of sextupole is large enough. The modulation of linear betatron motion by the synchrotron oscillation damages the momentum acceptance at resonances $2\nu_{x,y} \pm m\nu_z = N$. This resonance can be avoided either by careful choice of the operating point or by making the momentum compaction factor smaller with a π cell ring.

ACKNOWLEDGMENTS

We thank J. Irwin for useful comments. We also thank D. H. Whittum for help in writing the manuscript.

[1] K. L. Brown, IEEE Trans. Nucl. Sci. **NS-26**, 3490 (1979); K. L. Brown and R. Servranckx, in *Physics of High Energy Particle Accelerators (Brookhaven National Laboratory, Upton, New York and the State University of New York at Stony Brook),* Proceedings of the Third Annual U.S. Summer School on High Energy Particle Accelerators, AIP Conf. Proc. No. 127, edited by Melvin Month, Per F. Dahl, and Mrgaret Dienes (AIP, New York, 1983), p. 62.

[2] K. Oide, Nucl. Instrum. Methods A **276**, 427 (1989); J. Irwin, Nucl. Instrum. Methods A **298**, 460 (1990); O. Napoly, T. M. Taylor, and B. Zotter, Part. Accel. **30**, 137 (1990); J. Irwin, K. L. Brown, F. Bulos, D. L. Burke, R. H. Helm, G. Roy, R. D. Ruth, N. Yamamoto, and K. Oide, in *Proceedings of 1991 IEEE Particle Accelerator Conference, San Francisco, 1991,* edited by L. Lizama and J. Chew (IEEE, New York, 1991), p. 2058.

[3] R. Servranckx and K. L. Brown, IEEE Trans. Nucl. Sci. **NS-26**, 3598 (1979); A. Verdier, in *Proceedings of the 12th International Conference on High-Energy Accelerators, Fermi National Accelerator Laboratory, Batavia, Illinois, 1983,* edited by Francis T. Cole and Rene Donaldson (Fermi National Accelerator Laboratory, Batavia, IL, 1983), p. 173; L. Emery, in *Proceedings of the 1989 IEEE Particle Accelerator Conference, Chicago, 1989,* edited by Floyd Bennet and Joyce Kopta (IEEE, New York, 1989), p. 1225.

[4] See, e.g., A. Chao, in *Nonlinear Dynamics and Particle Acceleration, Tsukuba, Japan, 1990,* edited by Yoshi H. Ichikawa and Toshiki Tajima, AIP Conf. Proc. No. 230 (AIP, New York, 1990), p. 203; R. L. Warnock and R. D. Ruth, Phys. Rev. Lett. **66**, 990 (1991).

[5] E. D. Courant and H. S. Snyder, Ann. Phys. (N.Y.) **3**, 1 (1958).

[6] K. Oide, Nucl. Instrum. Methods A **276**, 427 (1989); K. Hirta, *Proceedings of the Second Advanced ICFA Beam Dynamics Workshop, Lugano, Switzerland, 1988,* edited by J. Hagel and E. Keil (European Organization for Nuclear Research, Geneva, Switzerland, 1988), p. 62.

[7] See, e.g., M. H. R. Donald, P. L. Morton, and H. Wiedemann, IEEE Trans. Nucl. Sci. **NS-24**, 1200 (1977); G. Guignard, *Nonlinear Dynamics Aspects of Particle Accelerators,* edited by J. M. Jowett, M. Month, and S. Turner, Lecture Notes in Physics Vol. 247 (Springer-Verlag, New York, 1985), p. 367; B. W. Montague, in *Proceedings of CERN Accelerator School Advanced Accelerator Physics, The Queen's College, Oxford, England, 1985, CERN 87-03,* edited by S. Turner (European Organization for Nuclear Research, Geneva, Switzerland, 1987), p. 85.

[8] E. Forest and J. Milutinovic, Nucl. Instrum. Methods A **269**, 474 (1988).

[9] M. Sands, *Physics with Intersecting Storage Rings,* edited by B. Touschek (Academic, New York, 1971), p. 257.

[10] T. Nishikawa *et al., TRISTAN, Electron-Positron Colliding Beam Project,* KEK Report No. 86-14 (National Laboratory for High Energy Physics, Tsukuba, Japan, 1987).